Eur. Phys. J. A **26**, 271–275 (2005)
DOI 10.1140/epja/i2005-10178-y

THE EUROPEAN PHYSICAL JOURNAL A

Mass distribution studies in the $^{19}F + ^{197}Au$ reaction

R. Tripathi and A. Goswami[a]

Radiochemistry Division, Bhabha Atomic Research Centre, Mumbai-400085, India

Received: 8 July 2005 / Revised version: 16 November 2005 /
Published online: 12 December 2005 –
Communicated by C. Signorini

Abstract. Mass distribution and evaporation residue measurements have been carried out in the reaction $^{19}F + ^{197}Au$ using the recoil catcher technique followed by off-line γ-ray spectrometry. The random neck rupture model (RNRM) has been used to compute the variance of the mass distribution (σ_A^2) and the average kinetic energy ($\overline{TKE}$) of the fission fragments for the present system. The results of model calculations have been found to be in good agreement with the experimental observations. Measured evaporation residue cross-sections have been compared with the statistical model calculations.

PACS. 25.70.Jj Fusion and fusion-fission reactions – 21.10.Gv Mass and neutron distributions – 24.75.+i General properties of fission

1 Introduction

Mass distribution is an important observable of the fission process. Studies on the mass distribution provide valuable information about the potential energy landscape of the fissioning nucleus and the mechanism involved [1,2]. A large amount of experimental data on the mass distribution in nuclear fission has been generated over the years. Early studies on low-energy fission of actinides revealed the importance of the nuclear shell effects in fission. The main interest in the medium-energy heavy-ion–induced fission is to study the effect of entrance channel parameters namely, projectile energy, angular momentum and entrance channel mass asymmetry, on the fission process. An analysis of the data on the variance of the mass distribution over a wide range of the fissility of the compound nucleus was reported in refs. [3,4]. The analysis revealed that the variance of the mass distribution decreases with the increase in fissility up to $Z^2/A \sim 34$ and then it increases [4]. Thus, the variance of the mass distribution provides important information about the fission process and can be used to test various models of fission such as the saddle point model [5] and the scission point model [6]. These models, although they qualitatively explain the gross features of the mass distribution, fail to quantitatively explain the mass distribution. Brosa *et al.* [7] proposed the random neck rupture model (RNRM) for the calculation of post-fission observables such as mass distribution, kinetic-energy distribution and neutron multiplicity. According to this model, the pre-scission shape of the fissioning nucleus dictates the post-fission observables. This model has been successful in explaining the width of the mass distribution in low- as well as medium-energy fission [7–10]. In the present work, mass distribution and evaporation residues were measured in the reaction $^{19}F + ^{197}Au$ at $E_{lab} = 96$ and 100 MeV using the recoil catcher technique followed by off-line γ-ray spectrometry. Experimentally determined variances of the mass distribution have been compared with those calculated using the RNRM of Brosa *et al.* [7]. The results of the evaporation residue (ER) measurement have been analysed in terms of statistical model.

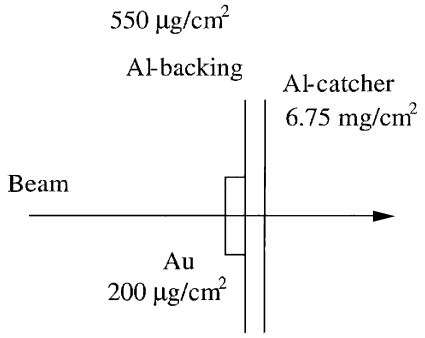

Fig. 1. Schematic drawing of the target-catcher assembly for the measurement of the mass distribution and evaporation residues in the $^{19}F + ^{197}Au$ reaction.

2 Experimental

Experiments were carried out using the ^{19}F beam from the 14 MV BARC-TIFR Pelletron accelerator, Mumbai, India. Targets were prepared by vacuum evaporation of

[a] e-mail: agoswami@apsara.barc.ernet.in

Table 1. Nuclear data (γ-ray energy, abundance and half-life) of the fission products and evaporation residues studied in the present work [11,12].

Nuclide	E_γ	Abundance (a_γ)	Half-life
^{91}Sr	749.8	23.6	9.52 h
^{92}Sr	1383.9	90	2.71 h
^{94}Y	918.8	73.3	18.6 min
^{95}Zr	756.7	55.4	64.03 d
^{97}Zr	657.9	106	17 h
^{98}Nb	787.4	93.0	51.3 min
^{99}Mo	140.5	90.7	2.75 d
^{103}Ru	497.1	89.5	39.25 d
^{105}Ru	724.2	46.7	4.44 h
^{107}Rh	302.8	66	21.7 min
^{111}Pd^{m}	172.2	33.5	5.5 h
^{111}Ag	342.1	6.7	7.45 d
^{112}Pd	606.7	3.60	21.05 h
^{117}Cd^{m}	158.6	109.	3.36 h
^{122}Sb	564	70.8	2.7 d
^{207}At	814.5	44.5	1.80 h
^{208}At	686.5	97.56	1.63 h

gold onto super-pure aluminium foil. The thickness of the gold layer was about 200 μg/cm^2. Irradiation was carried out with the gold layer facing the beam. A super-pure aluminium catcher having thickness 6.75 mg/cm^2 was kept after the target to stop the recoiling fission products. A schematic diagram of the target-catcher assembly is shown in fig. 1. Irradiation was carried out for about four hours at each beam energy. After irradiation, the target was used to estimate the ERs and the catcher was used for the assay of the fission products. The fission products and ERs were identified by their characteristic γ-rays. The nuclear data of the fission products and ERs used in the present work are given in the table 1 [11,12]. The γ-ray activity was assayed using a pre-calibrated HPGe detector connected to a PC-based 4k-channel analyzer. The resolution of the detector was 2.0 keV at 1332 keV of ^{60}Co. The decay of the fission products and ERs was followed for about one week. The activities of the fission products and ERs at the end of irradiation were used to arrive at the formation cross-sections using the standard activation equation [4].

3 Results and discussion

3.1 Mass distribution in the ^{19}F + ^{197}Au reaction

The yield of a mass chain $Y(A)$ is calculated using the experimentally determined independent yield *IN(A,Z)* or cumulative yield *CU(A,Z)* of the fission product with mass A and atomic number Z using the following equations:

$$Y(A) = IN\,(A,Z)\,/FIY\,(A,Z)\,, \tag{1}$$

$$Y(A) = CU\,(A,Z)\,/FCY\,(A,Z)\,, \tag{2}$$

where $FIY(A,Z)$ and $FCY(A,Z)$ signify the fractional independent and cumulative yields, respectively, of the fission product with mass number A and atomic number Z. $FIY(A,Z)$ and $FCY(A,Z)$ are given by the following equations:

$$FIY(A,Z) = \frac{1}{\sqrt{2\pi\sigma_z^2}} \int_{Z-0.5}^{Z+0.5} e^{-(Z-Z_p)^2/2\sigma_z^2} \mathrm{d}Z\,, \tag{3}$$

$$FCY(A,Z) = \frac{1}{\sqrt{2\pi\sigma_z^2}} \int_{-\infty}^{Z+0.5} e^{-(Z-Z_p)^2/2\sigma_z^2} \mathrm{d}Z\,. \tag{4}$$

Thus, the calculation of the mass yield for a mass chain with mass number A from the experimentally determined yield of a fission product requires the knowledge about the most probable charge Z_p for the mass chain and the width σ_Z of the isobaric yield distribution of the mass chain. The value of σ_Z was taken as 0.8 as determined in the ^{20}Ne + ^{208}Pb reaction at comparable excitation energy of the compound nucleus [4]. Based on the unchanged charge distribution (UCD) hypothesis, the Z_p value for a particular mass chain with mass number A was calculated using the following equation:

$$Z_p(A) = \frac{A}{(A/Z)_p}\,, \tag{5}$$

where $(A/Z)_p$ was calculated using the following equation:

$$(A/Z)_p = \frac{A_{cn} - \bar{\nu}_T}{Z_{cn}}\,, \tag{6}$$

where A_{cn} and Z_{cn} are the mass and atomic number of the compound nucleus, respectively. $\bar{\nu}_T$ is the average number of fission neutrons, which was calculated using the prescription of Kozuline *et al.* [13]. The Z_p values, calculated using the UCD hypothesis, were corrected for charge polarization using the prescription of W.J. Swiatecki [14]. These Z_p values were used to correct the experimentally determined yields to obtain the mass yields. The mass yields were also assigned to the masses of a complementary fission product with mass number $A_{cn} - \bar{\nu}_T - A$. For further discussion, these yields will be referred to as complementary fission product yields. The plots of mass yields in the ^{19}F + ^{197}Au reaction at E_{lab} = 96 and 100 MeV are shown in the lower and upper panels of fig. 2, respectively. In this figure, the experimentally determined mass yields are shown as filled symbols and the complementary fission product yields are shown as hollow symbols. The mass yields were fitted to a Gaussian function (shown as solid lines in the figure) to obtain the variance of the mass distribution. The excitation energies of the compound nucleus (E^*_{cn}) at E_{lab} = 96 and 100 MeV are about 52 and 55 MeV, respectively. The experimentally measured variances of the mass distribution in the present experiment are close to the values reported for the systems ^{16}O + ^{204}Pb, ^{16}O + ^{208}Pb at comparable excitation energy and fissility of the compound nucleus [15].

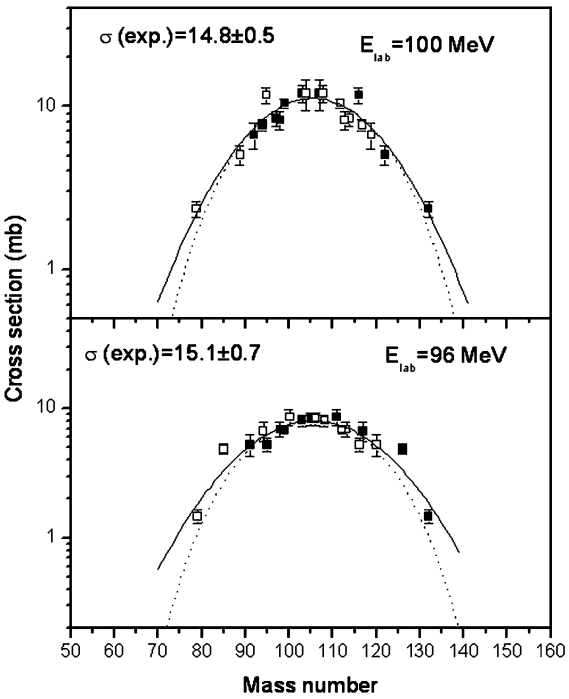

Fig. 2. Mass distribution in the reaction $^{19}F + ^{197}Au$. The filled symbols are the experimental points and the hollow symbols are the complementary points. The solid lines are Gaussian fit to the data and the dotted lines are the results of the RNRM calculation.

However, the experimentally measured values of the variance are found to be lower than that observed in the reaction $^{18}O + ^{197}Au$ [16] forming the compound nucleus ^{215}Fr which is close to the compound nucleus of the present system. The average angular momentum ($\langle l \rangle$) in the reaction $^{18}O + ^{197}Au$ [16] (= 49 $\hbar$) is much higher than that in the present experiment (= 19 and 23 $\hbar$ at E_{lab} = 96 and 100 MeV, respectively) resulting in higher fissility of the compound nucleus compared to that of the compound nucleus studied in the present work. The higher fissility of the compound nucleus may result in larger variance of the mass distribution as discussed in ref. [4]. In order to obtain the absolute cross-sections for various mass chains, the area under the Gaussian curve was normalized with respect to the absolute fission cross-section obtained from the measurement of the fission fragment angular distribution in the $^{19}F + ^{197}Au$ reaction [17].

In the present work, the RNRM of Brosa *et al.* [7] was used to calculate the width of the mass distribution. According to this model, during the motion of the fissioning nucleus towards scission, a dent is developed in the neck region of the fissioning nucleus, which is deepened by the capillary force, finally leading to fission. The curvature of the fissioning nucleus changes from positive to negative in the motion towards scission. During this transition when the neck becomes flat, there can be a large shift in the dent without sizeable physical mass motion, which finally leads to large mass fluctuations in fission. In the RNRM model [7] the pre-scission shape for the symmetric fission

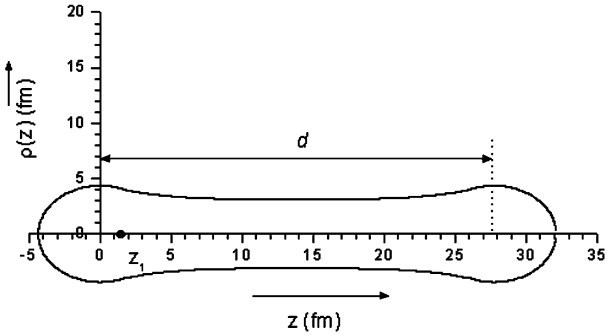

Fig. 3. Pre-scission shape of ^{216}Ra. The quantities shown in the figure are described in the text.

is described by the following set of equations:

$$\rho(z) = \begin{cases} \left(r_1^2 - z^2\right)^{1/2}, & r_1 \le z \le z_1, \\ r_2 + a^2 c \left(\cosh \frac{z - d/2}{a} - 1\right), & z_1 \le z \le d - z_1, \\ \left[r_1^2 - (d-z)^2\right]^{1/2}, & d - z_1 \le z \le d + r_1. \end{cases} \quad (7)$$

Equation (7) represents a shape which is made up of two equal spheres which are connected by a neck with minimal curvature c. This shape involves six parameters (r_1, z_1, r_2, a, c, d) (fig. 3). r_1 is the radius of the spherical heads at both ends of the pre-scission shape, r_2 is the minimal neck radius and z_1 is the transitional point where the function describing the shape changes. c is the curvature of the neck, where the neck is thinnest, *i.e.* at the geometrical centre of the shape in the case of symmetric pre-scission shape. The parameter a is a measure of the extension of the neck from the geometrical centre of the pre-scission shape, where the curvature is minimum, to the point where the curvature increases by a factor of 1.54. The total elongation L of the pre-scission shape is $d + 2r_1$. By imposing the conditions of continuity of the shape and volume conservation, a set of nonlinear equations was obtained. The equations were solved using the algorithms from ref. [18] to determine r_1, z_1 and a. The neck parameter r_2 was fixed by Rayleigh's instability criterion as given by the equation [7]

$$d - 2\widetilde{r}_1 = 4.5 r_2 \,, \quad (8)$$

where r_1 was calculated as $1.15(A_{cn}/2)^{1/3}$. The curvature c was calculated using the following equation [7]:

$$c = c_{rel} 8(\widetilde{r}_1 - r_2)/d^2 \,. \quad (9)$$

The value of c_{rel} was taken as 0.1 as used in ref. [7]. The remaining variable d was varied to reproduce the experimental variance of the mass distribution. For a given value of d, the pre-scission shape was determined and the probability of neck rupture at different positions of the neck (z_r) was calculated using the following equation [7]:

$$W(A) = \exp\left\{-2\pi\gamma_0 \left[\rho^2(z_r) - \rho^2(z)\right]/T\right\}, \quad (10)$$

where γ_0 is the surface tension coefficient given by

$$\gamma_0 = 0.9517\left[1 - 1.7828\left(\frac{N_{cn} - Z_{cn}}{A_{cn}}\right)^2\right] \mathrm{MeV\,fm^{-2}}\,. \tag{11}$$

N_{cn} and Z_{cn} are the neutron number and atomic number of the fissioning nucleus and T is the temperature of the fissioning nucleus at the scission point. The temperature T at the scission point was calculated using the following equation:

$$T = \sqrt{E^*_{scission}/a}\,, \tag{12}$$

where $E^*_{scission}$ is the excitation energy of the fissioning nucleus at the scission point. In view of the large excitation energy of the compound nucleus (E^*_{cn}), E^*_{cn} was approximated as $E^*_{scission}$. The level density parameter a was taken as $A/8\,\mathrm{MeV}^{-1}$. The rupture position (z_r) was translated into the fragment mass using the following relation:

$$A(z_r) = \frac{3A_{cn}}{4r^3_{cn}} \int_{-r_1}^{z_r} \rho^2(z)\mathrm{d}z\,. \tag{13}$$

The variance of the mass distribution σ^2_A was calculated using the following equation:

$$\sigma^2_A = \frac{\sum\limits_A \left(A - A_{cn}/2\right)^2 W\left(A\right)}{\sum W\left(A\right)}\,. \tag{14}$$

Fission masses were corrected for the number of fission neutrons $\bar{\nu}_T$ as calculated using the prescription of Kozuline *et al.* [13]. The $\bar{\nu}_T$ value was apportioned in the mass ratio of the fission fragments for the correction. The total elongation of the pre-scission length L which reproduced the experimental variance for the present system was found to be 36.5 fm. This value of L was used to calculate the $\overline{\mathrm{TKE}}$ using the prescription given in refs. [7,8]. The calculated value of $\overline{\mathrm{TKE}}$ was found to be in good agreement with the experimentally determined value reported in ref. [19].

The deformation energy of the fissioning nucleus ^{216}Ra was calculated to locate the scission point in the exit channel using the procedure of Brack *et al.* [20]. In this procedure, the shape of the nucleus is described by three parameters, namely, the elongation parameter c, the neck parameter h and the asymmetry parameter α. The shape of the nucleus is expressed by the following equation [20]:

$$\begin{aligned} \nu^2_s &= \left(1 - u^2\right)\left(A + Bu^2 + \alpha u\right)\,, \qquad (B \geqslant 0)\,, \\ \nu^2_s &= \left(1 - u^2\right)\left(A + \alpha u\right) e^{\left(Bc^3u^2\right)}\,, \qquad (B < 0)\,. \end{aligned} \tag{15}$$

The shape will always have its end points at $u = \pm 1$. The relation between the parameter sets $\{A, B\}$ and $\{c, h\}$ is given by

$$\begin{aligned} B &= 2h + 0.5\left(c - 1\right)\,, \\ A &= \left(1/c^3\right) - 0.2B\,. \end{aligned} \tag{16}$$

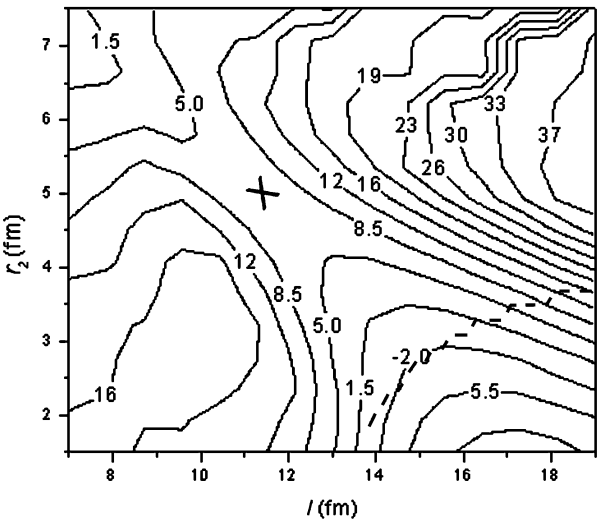

Fig. 4. Contour plot of the deformation energy of ^{216}Ra as a function of l and r_2. X marks the saddle point. The scission line is shown as dashed line.

The semi-length l ($= L/2$) in the parameterization of Brosa *et al.* [7] is related to the elongation parameter c by the following equation:

$$c = l/R_{cn}\,, \tag{17}$$

where R_{cn} is the radius of the fissioning nucleus in its spherical ground state. As the pre-scission shape is symmetric, the neck is thinnest at the geometrical centre of the shape, *i.e.* at $u = 0$ in the parameterization of Brack *et al.* [20]. By substituting ν_s by r_2/c and $u = 0$ in eq. (15), the following relation between the neck radius r_2 and h is obtained:

$$h = 2.5\Big[\left(1/c^3\right) - \left(r_2/c\right)^2 - 0.1\left(c - 1\right)\Big]\,. \tag{18}$$

Using eqs. (17) and (18), the coordinates (l, r_2) were transformed into the coordinates (c, h) for the calculation of the potential energy. In the present calculations, only the liquid-drop potential energy was considered, thus the asymmetry parameter α was taken as zero, which is valid for the symmetric pre-scission shape. A contour plot of the potential energy of the fissioning nucleus ^{216}Ra as a function of l and r_2 is shown in fig. 4. The saddle point is marked by a cross (X) in the figure. The scission line was calculated using the following criterion from ref. [20]:

$$\rho_{cm} \approx 1.16R_0\,, \tag{19}$$

where ρ_{cm} is half the distance between the centers of mass of the two halves of the nucleus. The scission line is shown as dashed line in fig. 4. The elongation of the pre-scission shape corresponding to the minimum potential energy is about 31 fm. However, this elongation results in a smaller variance in the RNRM calculation. As the RNRM calculation does not give a clear recipe for the location of the scission point [9], a critical calculation of the LDM parameters may be necessary to arrive at the elongation parameter, which reproduces the variance of the mass distribution using the RNRM calculation.

Table 2. Calculated and experimental evaporation residue cross-sections in the $^{19}F + ^{197}Au$ reaction.

E_{lab} (MeV)	σ_{ER} (mb)	
	Experimental (4n + 5n)	CASCADE calculation ($a_f/a_n = 1.065$)
96	28 ± 2	27
100	34 ± 4	30

3.2 Evaporation residue measurement in the $^{19}F + ^{197}Au$ reaction

In the present work, the formation cross-section of At isotopes was determined from their γ-ray activity using the standard activation equation. The cross-section of At isotopes was used to calculate the cross-sections of Ra isotopes using the following equations:

$$\sigma_{^{211}\mathrm{Ra}} = 1.265\,\sigma_{^{207}\mathrm{At}}\,, \qquad \sigma_{^{212}\mathrm{Ra}} = 2.597\,\sigma_{^{208}\mathrm{At}}\,. \tag{20}$$

The coefficients in the equation are correction factors for the partial decay of Ra isotopes to At isotopes. The branching fractions for the partial decay of Ra isotopes to At isotopes were taken from ref. [12]. The formation cross-sections of the Ra isotopes are given in table 2. The uncertainties quoted on the formation cross-section are the standard deviation of the multiple counting reflecting the uncertainty due to counting statistics. However, the overall uncertainty on the formation cross-sections of evaporation residues will be higher due to the contribution from systematic errors, mainly the error in the detection efficiency and uncertainty in the target thickness. In the present experiment, the efficiency calibration of the detector has been carried out in the energy region from 121 to 1408 keV using the standard ^{152}Eu source. The efficiency error in this energy region is within 2–7%; however, the efficiency error at the energies of the γ-rays which have been used for the residue measurement, is within 2–4%. The uncertainty in the target thickness is about 5%. The formation cross-sections of the Ra isotopes were calculated using the code CASCADE [21]. The fusion cross-sections and spin distributions of the compound nucleus were calculated using the code CCFUS [22] and supplied as input parameters for the CASCADE calculation. The calculated fusion cross-section at $E_{lab} = 96$ and 100 MeV was 266 and 395 mb, respectively, corresponding to a L_{fus} value of 29 and 35 $\hbar$, respectively. The CASCADE calculations reproduced the measured ER cross-section with the value of a_f/a_n as 1.065. In the CACADE calculation, 4n and 5n emission channels account for the almost entire cross-section of the ERs and the remaining fusion cross-section is for fission. The calculated ER cross-sections are given in table 2. As fission-evaporation competition strongly depends on a_f/a_n, it was difficult to conclude about the fusion probability on the basis of the ER cross-section.

4 Conclusions

Mass distributions were measured in the $^{19}F + ^{197}Au$ reaction. The variance of the mass distribution was computed using the RNRM. In RNRM calculations, the elongation of the pre-scission shape was varied to reproduce the experimental variance of the mass distribution. The $\overline{\mathrm{TKE}}$ value calculated using this elongation was found to be in reasonably good agreement with the experimental value reported in the literature. However, the calculation of the deformation energy of the fissioning nucleus reveals a less elongated pre-scission shape.

Evaporation residue cross-sections were measured and compared with the statistical model calculations. Evaporation residue cross-sections could be reproduced by the CASCADE calculations with the a_f/a_n value of 1.065.

References

1. R. Vandenbosch, J.R. Huizenga, *Nuclear Fission* (Academic Press, Inc., New York, 1973).
2. C. Waggemans, *The Nuclear Fission Process* (CRC, London, 1991).
3. A.Ya. Rusanov, M.G. Itkis, V.N. Okolovich, Z. Phys. A **342**, 299 (1997).
4. R. Tripathi, K. Sudarshan, A. Goswami, P.K. Pujari, B.S. Tomar, S.B. Manohar, Phys. Rev. C **69**, 024613 (2004).
5. C.F. Tsang, J.B. Wilhelmy, Nucl. Phys. A **184**, 417 (1972).
6. B.D. Wilkins, E.P. Steinberg, R.R. Chasman, Phys. Rev. C **14**, 1832 (1976).
7. U. Brosa, S. Grossmann, Z. Phys. A **310**, 177 (1983).
8. Ulrich Brosa, Siegfried Grossmann, Andreas Müller, Phys. Rep. **197**, 167 (1990).
9. M.C. Duijvestijn, A.J. Koning, F.J. Hambasch, Phys. Rev. C **64**, 014607 (2001).
10. I.V. Pokrovsky *et al.*, Phys. Rev. C **62**, 014615 (2000).
11. U. Reus, W. Westmeier, At. Data Nucl. Data Tables **29**, 1 (1983).
12. R.B. Firestone, V.S. Shirley, *Table of Isotopes*, 8th edition, Vol. **I** (John Wiley & Sons, Inc., New York, 1996).
13. E.M. Kozuline, A.Ya. Rusanov, G.N. Smirenkin, Phys. At. Nucl. **56**, 166 (1993).
14. W.J. Swiatecki, J. Phys. (Paris) **33,** C5-45 (1972).
15. M.G. Itkis, Yu. Ts. Oganessian, G.G. Chubarian *et al.*, *European Division Conference: Low Energy Nuclear Dynamics*, edited by Yu.Ts. Oganessian (World Scientific, Singapore, 1995) p. 177.
16. D.J. Hinde, D. Hilscher, H. Rossner, B. Gebauer, M. Lehmann, M. Wilpert, Phys. Rev. C **45**, 1229 (1992).
17. R. Tripathi, K. Sudarshan, S. Sodaye, A.V.R. Reddy, K. Mahata, A. Goswami, Phys. Rev. C **71**, 044616 (2005).
18. W.H. Press, S.A. Teukolsky, W.T. Vellerling, B.P. Flannery, *Numerical Recipes in FORTRAN*, 2nd edition (Cambridge University Press, 1992).
19. A.Yu. Chizhov *et al.*, Phys. Rev. C **67**, 011603 (2003).
20. M. Brack, Damgaard Jens, A.S. Jensen, H.C. Pauli, V.M. Strutinsky, C.Y. Wong, Rev. Mod. Phys. **44**, 320 (1972).
21. F. Puhlhofer, Nucl. Phys. A **280**, 267 (1977).
22. C.H. Dasso, S. Landowne, Comput. Phys. Commun. **46**, 187 (1987).